Published in final edited form as:
*Nat Med*. 2010 May ; 16(5): 535–143. doi:10.1038/nm.2144.

# Epithelial cell cycle arrest in G2/M mediates kidney fibrosis after injury

**Li Yang**[1,2], **Tatiana Y Besschetnova**[1,3], **Craig R Brooks**[1], **Jagesh V Shah**[1,3,4], and **Joseph V Bonventre**[1,4]

[1]Renal Division, Brigham and Women's Hospital, Department of Medicine, Harvard Medical School, Boston, Massachusetts, USA

[2]Renal Division, Department of Medicine, Peking University First Hospital, Beijing, China

[3]Department of Systems Biology, Harvard Medical School, Boston, Massachusetts, USA

[4]Harvard–Massachusetts Institute of Technology, Division of Health Sciences and Technology, Cambridge, Massachusetts, USA

## Abstract

Fibrosis is responsible for chronic progressive kidney failure, which is present in a large number of adults in the developed world. It is increasingly appreciated that acute kidney injury (AKI), resulting in aberrant incomplete repair, is a major contributor to chronic fibrotic kidney disease. The mechanism that triggers the fibrogenic response after injury is not well understood. In ischemic, toxic and obstructive models of AKI, we demonstrate a causal association between epithelial cell cycle G2/M arrest and a fibrotic outcome. G2/M-arrested proximal tubular cells activate c-jun $NH_2$-terminal kinase (JNK) signaling, which acts to upregulate profibrotic cytokine production. Treatment with a JNK inhibitor, or bypassing the G2/M arrest by administration of a p53 inhibitor or the removal of the contralateral kidney, rescues fibrosis in the unilateral ischemic injured kidney. Hence, epithelial cell cycle arrest at G2/M and its subsequent downstream signaling are hitherto unrecognized therapeutic targets for the prevention of fibrosis and interruption of the accelerated progression of kidney disease.

The repair process after tissue injury involves a regeneration phase, in which injured cells are replaced by cells of the same lineage[1], and a fibrotic phase, in which connective tissues replace normal parenchymal tissue[2]. Repair can either leave no lasting evidence of damage or can result in fibrotic lesions that can lead to progressive organ dysfunction. In the kidney, fibrosis is responsible for chronic progressive kidney failure, which is present in approximately 8–10% of individuals in the developed world[3,4]. AKI can result in incomplete repair and persistent tubulointerstitial inflammation, with proliferation of fibroblasts and excessive deposition of extracellular matrix, a common feature of many kinds of kidney diseases and a primary determinant of progression to end-stage renal failure[5,6]. The cellular



Correspondence should be addressed to J.V.B. (joseph_bonventre@hms.harvard.edu).

Note: Supplementary information is available on the Nature Medicine website.

**Author Contributions**: L.Y. and J.V.B. designed the experiments and wrote the manuscript. L.Y. performed experiments and collected and analyzed data. J.V.B. supervised the project. J.V.S. designed the *in vitro* rescue experiment and advised on cell biology. T.Y.B. helped collect data and edited the manuscript. C.R.B. helped with making lentivirus shRNA specific for ATM. All authors discussed the results and implications and commented on the manuscript.

**Competing Financial Interests**: The authors declare no competing financial interests.

mechanisms that facilitate tubulointerstitial fibrosis after injury remain poorly defined. Whereas tubular epithelial cells have been proposed to have an active role in the progression of fibrosis via epithelial-to-mesenchymal transformation[7–9], recent data indicate that fibrosis can occur in the absence of this cellular transformation process[1,10]. It also has been proposed that profibrotic factors such as transforming growth factor-β1 (TGF-β1) and connective tissue growth factor (CTGF) are upregulated in the tubulointerstitial area upon injury, leading to kidney fibrosis[11,12]. Currently, however, it is not clear how and to what extent tubular cells contribute to tissue fibrosis.

The potent capacity of tubular epithelial cells to proliferate and replace lost cells is crucial for repair and enables recovery from many ischemic or toxic insults[1,13]. Enhanced expression of cell cycle regulatory proteins such as p53, p21 and p16 in renal proximal tubular cells has been implicated in repair in ischemic and cisplatin-toxic AKI animal models, deteriorating renal transplants and chronic-diseased native kidneys in human beings[14–17]. There is increasing evidence that modulating these cell cycle regulatory proteins can affect the severity of acute ischemic or cisplatin-induced toxic kidney injury[18–20]. Cell cycle arrest or dysregulation, however, has not been linked to fibrosis. Here we characterized the cell cycle profile of tubular epithelial cells *in vivo* at various times after an acute insult in five AKI models: moderate reversible ischemia reperfusion injury (IRI), severe IRI, unilateral IRI, acute aristolochic acid toxic nephropathy (AAN) and unilateral ureteral obstruction (UUO). These models reflect three of the most common causes for AKI seen in humans: ischemia, toxic exposure and obstruction. Each is characterized by acute tubular injury and interstitial inflammation but have distinct long-term outcomes. The development of fibrosis and the production of profibrotic cytokines in each of the AKI models correlated with the arrest of proximal tubule epithelial cells in G2/M. Abrogating the G2/M arrest markedly reduced fibrosis and cytokine production, consistent with a direct role for cell cycle dysregulation in the progression of AKI to chronic kidney disease.

## Results

### Different fibrotic outcomes in various AKI models

To test the effect of injury on initiation and development of fibrosis in the kidney, we studied five AKI mouse models. We measured serum creatinine to evaluate renal dysfunction, as it is a measure of glomerular filtration rate. The normal serum creatinine concentration in mice is below 0.2 mg $dl^{-1}$. The moderate IRI, severe IRI and AAN mice showed abrupt renal dysfunction after ischemia or aristolochic acid injection, with serum creatinine peaking at 1.50 ± 0.52 mg $dl^{-1}$, 2.40 ± 0.41 mg $dl^{-1}$ and 1.02 ± 0.21 mg $dl^{-1}$, respectively (Fig. 1a). In the moderate IRI model, serum creatinine decreased sharply after the peak on day 1 and returned to normal levels by day 7 (Fig. 1a). In the severe IRI and AAN mouse models, however, the decrease in serum creatinine was delayed, and serum creatinine remained above normal levels for at least 42 d after injury ($P < 0.01$, Fig. 1a) and did not return to baseline for the duration of the study. In the two unilateral AKI models, the unilateral IRI and UUO models, the serum creatinine concentration did not increase significantly because of compensation by the normal contralateral kidney (Fig. 1a).

In all models other than moderate IRI, histological examination revealed interstitial fibrosis (Fig. 1b), which was confirmed by tissue collagen quantification (Fig. 1c). Immunostaining of markers associated with fibrosis including collagen I V, α-smooth muscle actin (α-SMA) (Fig. 1d) and collagen I together with morphometric quantification (Fig. 1e) revealed robust protein accumulation in the interstitial area, demonstrating the chronic fate of the kidney in the four AKI models.

### Tubular G2/M arrest characterizes profibrotic AKI models

The cellular hallmark of kidney repair after AKI is a proliferative response of surviving tubular epithelial cells. In all of the AKI models, there was prominent renal tubule proliferation after acute injury. The cell cycle distribution *in vivo* during injury and recovery was characterized as a function of time in moderate IRI, unilateral IRI, AAN, severe IRI and UUO models (Fig. 2a–c).

To analyze the cell cycle distribution of proximal tubular epithelial cells *in vivo*, we used several approaches. We complemented immunohistochemistry staining of cell cycle markers *in vivo* with analysis of cell cycle markers in isolated proximal tubules, and we compared chromatin characteristics *in vivo* with chromatin pattern at various stages of the cell cycle *in vitro*. We labeled proliferating cells (G1, S, G2 and M phase) *in vivo* with Ki-67 specific antibody[21] (Fig. 2a), identified cells in S phase by the uptake of BrdU, detected by staining with antibody to BrdU[21] (Fig. 2a) and detected cells in G2/M phase by quantifying the number of tubular cells with phosphorylation of histone H3 at Ser10 (p-H3) through staining with a phosphorylation-specific antibody[22] (Fig. 2a). As demonstrated by flow cytometry analysis, p-H3 was also a good marker for the G2/M phase of the cell cycle *in vitro* (Supplementary Fig. 1a). Immunostaining of p-H3 in cells *in vitro* (Supplementary Fig. 1a,b) and in tissues *in vivo* (Supplementary Fig. 1c) revealed the same staining patterns in the G2 and M stages of the cell cycle. We calculated the number of cells in G1 phase by subtracting the number of cells in S phase (BrdU positive) and G2/M phase (p-H3 positive) from the total number of proliferating cells (Ki-67 positive) and expressed the proportion of cells in each phase as the percentage of total proliferating cells (Fig. 2b,c).

The moderate IRI mice had transient cell cycle changes in proximal tubular cells in the outer medulla (Fig. 2a,b), with a high proportion of S phase (65.2 ± 6.8%) on day 1, reflecting an active repair response. The percentage of cells in G2/M phase increased from approximately 15% on day 1 to 30% on day 5 (Fig. 2b). After day 7, the cell cycle distribution of proliferating tubular cells reached a relatively stable profile, with approximately 15–20% in S phase and 15–20% in G2/M phase (Fig. 2b). The unilateral IRI model mice showed a similar initial proximal tubular proliferation curve when compared to the moderate IRI mice (Fig. 2a,b); however, the percentage of cells in G2/M phase increased to greater than 50% by day 5 and remained at a high level for the duration of observation (82.2% ± 10.9% on day 42, Fig. 2b). In the AAN model, there was an increase in cortical proximal tubular cells in S phase, peaking at day 14, with a subsequent reduction in S phase cells to 15–20% after 28 d (Fig. 2a,b). Similar to the unilateral IRI model, there was an obvious and persistent higher number of cells in G2/M phase beginning from day 5 and remaining at high levels during the entire repair phase (56.6% ± 5.9% on day 42, Fig. 2b). Thus, in the unilateral IRI and AAN AKI models, which both resulted in fibrosis, the common feature was the increase in a persistent proximal tubule G2/M population (Fig. 2b,c). The findings in the UUO and severe bilateral IRI were similar to the unilateral IRI and AAN models, with G2/M populations accumulating from day 3 through day 28 or day 14, respectively (Fig. 2c).

The cells that co-stained with antibodies to Ki-67 and p-H3 in kidneys examined 7 d after unilateral IRI were tubular cells (Fig. 2d). The co-staining reflected a much higher proportion of cells in the G2/M phase of the cycling population in unilateral IRI when compared to moderate IRI. By co-staining of proliferative markers and proximal tubular markers (lotus lectin[23] (data not shown) and Kim-1[24], Fig. 2e), we found that more than 95% of the proliferating tubular cells after acute injury from ischemia-reperfusion, aristolochic acid treatment or UUO were of proximal tubular origin. Accumulation of cells in G2/M in models of AKI associated with fibrosis was also confirmed by the increased cyclin B1/cyclin D1 ratio, seen in severe IRI, unilateral IRI, AAN and UUO (Fig. 2f).

Furthermore, we characterized the time-dependence of BrdU incorporation in AKI models (Fig. 2g,h). We injected mice with BrdU to label cells in S phase and removed kidneys at 2, 4, 8 and 12 h after BrdU injection (Fig. 2g). At later time points, there were very few BrdU-positive cells in the moderate IRI kidney that co-stained with p-H3 (Fig. 2g,h), indicating that cells that labeled with BrdU had progressed through the cell cycle and past the G2/M phase. By contrast, in the profibrotic kidney models (AAN and UUO), most of the tubular cells that took up BrdU were still in G2/M phase of the cell cycle 4, 8 and 12 h later, indicating that the increase in number of tubular cells in G2/M in the profibrotic AKI models is due to the elongation of the G2/M phase in these cells (Fig. 2g,h). We did not detect G2/M arrest in the interstitial cells in any of the AKI models (data not shown). Thus, all AKI mouse models where prominent fibrosis developed (unilateral IRI, severe IRI, AAN and UUO), are characterized by arrest of proximal tubular epithelial cells in the G2/M phase of the cell cycle. To verify whether G2 or M phase arrest was more characteristic of the observed fibrotic phenotype, we used the characteristics of p-H3 staining to distinguish G2 from prophase and late mitotic phases[22,25]. We found that about 95% of tubular cells were arrested in G2 phase, as observed by a typical G2 phase foci-like staining of p-H3 (Supplementary Fig. 1c).

## G2/M arrest results in upregulation of profibrogenic growth factors

To investigate whether and how proximal tubular epithelial cell arrest in G2/M is involved in fibrogenesis, we complemented studies *in vivo* with evaluation of the effects of aristolochic acid *in vitro* on several proximal tubular cell lines: human HK-2 cells, pig LLC-PK1 cells and rat IRPTC cells. In each of the cell lines, aristolochic acid (5 $\mu$g ml$^{-1}$) treatment for 48 h resulted in a marked increase in the percentage of cells in G2/M (Fig. 3a) and a marked upregulation of messenger RNA expression of fibrogenic growth factors encoding TGF-$\beta$1 and CTGF (Fig. 3b). In addition, aristolochic acid resulted in activation of the *COL4A1* gene (encoding collagen-4$\alpha$1) in HK-2 cells and IRPTC cells and *COL1A1* (encoding collagen-1$\alpha$1) in HK-2 cells (Fig. 3b). The protein amounts of TGF-$\beta$1 and CTGF were also increased in the supernatant of aristolochic acid –treated HK-2 cells by factors of 2.01 ± 0.23 ($P < 0.01$) and 39.94 ± 5.69 ($P < 0.001$), respectively (Fig. 3c).

To determine whether the G2/M cells were responsible for the generation of profibrotic factors, we isolated G0/G1 phase and G2/M phase cells by cell sorting using Hoechst staining. In normal cultured HK-2 cells, the G2/M phase cells had higher mRNA levels of *COL4A1* and *ACTA2* (encoding $\alpha$-smooth muscle actin, $\alpha$-SMA) than did cells in the G0/G1 phase, whereas the levels of *TGFB1* and *CTGF* were similar between the cells in the two phases of cell cycle (Fig. 3d). After aristolochic acid treatment for 48 h, HK-2 cells in both G0/G1 and G2/M phases showed a higher level of *TGFB1* gene production compared with the normally growing cells in the corresponding cell cycle phases (by factors of 2.01 ± 0.66 and 3.33 ± 0.48, respectively, $P < 0.05$) (Fig. 3d). HK-2 cells arrested in G2/M phase secondary to aristolochic acid exposure had elevated *CTGF* mRNA levels (6.0 ± 1.11 fold compared with normal cycling G2/M cells, $P < 0.01$) (Fig. 3d). HK-2 cells arrested in G2/M phase also showed increased levels of *COL4A1* and *ACTA2* gene production compared with G0/G1 phase cells in normal culture or after aristolochic acid treatment, but these levels were no higher than the normally cycling HK-2 cells in G2/M (Fig. 3d). Providing further evidence of a causal relationship between the profibrotic factors generated by the G2/M-arrested cells and fibrosis, we found that the conditioned medium from aristolochic acid–treated HK-2 cells enhanced proliferation (Fig. 3e) and collagen production (Fig. 3f) of fibroblasts *in vitro*.

We determined *in vivo* mRNA levels of *Tgfb1*, *Ctgf*, *Col4a1* and *Col1a1* in injured mouse kidney tissue of all models of AKI. Each of the AKI models showed elevated mRNA levels

of these four profibrogenic factors soon after the initiation of the injury (Fig. 3g). In the moderate IRI model, where fibrosis did not occur, the mRNA levels of these fibrogenic genes fell to baseline within the first 1 to 2 weeks after the acute insult, whereas in the other four AKI models, characterized by the development of fibrosis, elevated gene expression levels were sustained for 42 d or for the duration of the study (14 d in the case of UUO) (Fig. 3g).

In addition, TGF-β1 and CTGF protein production from tubules isolated from moderate IRI and aristolochic acid–treated mice were increased, as determined by western blot analysis, particularly in the aristolochic acid–treated group (Fig. 3h). TGF-β1 and CTGF co-localized with p-H3–positive tubular nuclei *in vivo* (Fig. 3i). Thus, profibrogenic growth factors are upregulated in G2/M-arrested tubular cells both *in vitro* and *in vivo*, and the factors produced *in vitro* can stimulate the proliferation and collagen production of fibroblasts.

Tubular cell apoptosis has been associated with fibrosis. In the present study, all of the AKI models, whether resulting in fibrosis or not, showed a substantial increase in tubular cell apoptosis after injury (Supplementary Fig. 2a). Furthermore, there were no differences in total integrated amount of apoptosis in the nonfibrotic moderate IRI model and the profibrotic AAN model over 42 d of observation after injury (Supplementary Fig. 2b). Over the first 14 d, there was more apoptosis in moderate IRI than in the aristolochic acid–treated mice, yet there was much more profibrogenic gene expression and protein production, as well as increased amounts of fibrosis, in the aristolochic acid–treated mice. The density of tubular cells *in vivo* supports the conclusion that G2/M arrest of epithelial cells affects the epithelial cell proliferating efficiency after an acute injury insult (Supplementary Fig. 2c). *In vitro*, aristolochic acid, at a dose of 5 $\mu g\ ml^{-1}$, upregulated profibrotic genes but did not cause enhanced apoptosis in HK-2 cells (Supplementary Fig. 2d). These data *in vivo* and *in vitro* suggest that epithelial G2/M arrest results in fibrosis independent of effects on apoptosis. The reduced number of epithelial cells seen in the injury models associated with fibrosis is therefore explained by cell cycle arrest rather than an increase in apoptosis.

## Reversal of G2/M arrest rescues the fibrogenic effect

G2/M checkpoint arrest occurs primarily through the activation of protein kinases Chk1 and Chk2, which are downstream of the ATM-ATR (ataxia telangiectasia, mutated–ATM and Rad3-related) pathway[26,27]. Although it has been well established that the ATM-ATR pathway can be activated by DNA damage, activation also occurs under non DNA-damaging conditions, such as hypoxia and reoxygenation[28]. We detected distinct ATM activation in the tubular cells in severe IRI, unilateral IRI, AAN and UUO mice through immunostaining of phosphorylated ATM ser1981 (p-ATM) (Fig. 4a and Supplementary Fig. 3a). There was no detectable p-ATR by either immunostaining or western blotting in control or kidney injury models (data not shown). In aristolochic acid–treated HK-2 cells, activation of the ATM pathway was also evident, as determined by immunostaining of p-ATM (Supplementary Fig. 3b) and western blot analysis of p-ATM, p-Chk2 and p-p53 (Fig. 4b). Incubating HK-2 cells with KU-55933 (an ATM inhibitor)[29] reduced the fraction of cells in G2/M arrest by ∼50% (Fig. 4c). Associated with the reduction in G2/M arrested cells, the mRNA levels of *TGFB1*, *CTGF*, *COL4A1* and *COL1A1* were also downregulated by ∼50% (Fig. 4c). We observed a similar rescue effect in LLC-PK1 cells and IRPTC cells treated with KU-55933 and aristolochic acid (Fig. 4c). We further confirmed the effect of ATM inhibition in reducing G2/M arrest and decreasing profibrogenic factor production by reducing ATM expression with shRNA in HK-2 cells and LLC-PK1 cells (Fig. 4d and Supplementary Fig. 3c). There were marked reductions in TGF-β1 and CTGF mRNA levels in both cell types when the we used ATM-specific shRNA to mitigate the effect of aristolochic acid on the number of cells in G2/M (Fig. 4d).

To further evaluate whether there is a causal relationship between G2/M arrest and fibrosis, we designed two experimental mouse models to rescue G2/M arrest. Both experiments were performed in the unilateral IRI model, which normally results in the development of prominent fibrotic lesions (Fig. 1b–e). One group of unilateral IRI mice was injected intraperitoneally with 2.2 mg per kg body weight of pifithrin-α (PIF-α), a p53 inhibitor[30], on days 3 and 14 after surgery. We injected control mice with the same amount of the saline vehicle. Another group of unilateral IRI mice underwent nephrectomy of the healthy contralateral kidney 3 d after unilateral IRI surgery. Both PIF-α treatment and contralateral nephrectomy decreased the accumulation of G2/M-arrested tubular cells by >50% and >60%, respectively, on day 10 after unilateral IRI (Fig. 4e). The degree of increase of mRNA levels of profibrogenic genes and the degree of interstitial fibrosis were all markedly reduced by either treatment (Fig. 4f,g). Given that we performed PIF-α injection or nephrectomy 3 d after unilateral IRI surgery, the severity of initial kidney injury was not affected by these treatments (by histological injury scoring, data not shown). Taken together, these data indicate that the development of fibrosis was markedly suppressed when the number of tubular epithelial cells arrested in G2/M was reduced *in vivo*.

As in the case of PIF-α treatment, at 42 d after unilateral IRI, the nephrectomy treatment group had much less fibrosis and less of an increase in kidney collagen content (Fig. 4g). The fibrosis that did exist was localized in focal stripe–like distributions (Fig. 4g). Although most of the tubular cells in this group showed no Ki-67 staining at 42 d, tubular cells on the edge of fibrotic tissue were still in an active proliferating status, with a marked increase in G2/M arrest in cells adjacent to the focal regions of deposition of collagen IV (Supplementary Fig. 3d).

## Imposed prolonged G2/M arrest causes a profibrotic phenotype

To further establish that prolonged arrest at the G2/M boundary can result in a prominent profibrotic phenotype we adopted alternative strategies to induce G2/M arrest. When we administered R03306, a cyclin-dependent kinase-1 inhibitor known to induce a reversible G2/M transition defect[31], to HK-2 and LLC-PK1 cells, the number of cells in G2/M increased to 30% at 24 h and ∼55–71% at 48 h (Fig. 5a,b). Profibrogenic gene expression was markedly increased at 48 h (Fig. 5b). Through Hoechst staining and cell sorting, we isolated the G2/M phase HK-2 cells after treatment with R03306 for 48 h and compared gene expression with that in G0/G1 cells. We confirmed the G2/M phase cells to be the origin of profibrogenic gene expression (Fig. 5c). After we washed out the R03306, the tubular cells were able to exit G2/M arrest, with a return of profibrogenic gene expression to close to baseline (Fig. 5b,c).

We also used paclitaxel (Taxol), a microtubule stabilizing agent[32], to induce progressive G2/M arrest. Low-dose (∼50 nM–10 μM) paclitaxel treatment of HK-2 cells for 24 h caused prominent G2/M arrest (Fig. 5d), with upregulation of mRNA expression of *TGFB1*, *CTGF*, *COL4A1* and *COL1A1* and increased CTGF protein secretion into the supernatant (Fig. 5e). Paclitaxel administration (20 mg per kg body weight) *in vivo* at 1 and 4 d after ischemia-reperfusion to the moderate IRI mice caused a sustained increase in the number of renal tubular cells in the G2/M phase (Fig. 5f) and, as predicted, resulted in development of interstitial fibrosis (Fig. 5g). To confirm that the observed phenotype was not the consequence of direct paclitaxel-induced tubular cell toxicity, we evaluated the serum creatinine concentration and the extent of tubular necrosis after paclitaxel administration. There were no differences in the peak serum creatinine concentration (Fig. 5h) or the degree of tubular necrosis (data not shown) between the moderate IRI and paclitaxel-treated moderate IRI mice.

### JNK signaling mediates fibrogenic cytokine upregulation

Given the well-known effect of mitogen-activated protein kinases (MAPKs) in cell proliferation, apoptosis and fibrosis, we evaluated their involvement in the fibrogenic effect caused by G2/M arrest. After treatment of HK-2 cells with aristolochic acid, R03306 or paclitaxel, there was prominent activation of JNK signaling, with increased levels of p-JNK and p–c-jun, that coincided with periods when G2/M arrest was prominent (Fig. 6a). We also found extracellular signal–regulated kinase (ERK) activation in HK-2 cells with each of the three treatments, but it occurred earlier than the onset of G2/M arrest (Fig. 6a). The level of p-p38 was increased with aristolochic acid or RO3306 treatment but not with paclitaxel treatment (Fig. 6a).

To investigate whether MAPKs might be mechanistically involved in G2//M arrest and profibrogenic gene production, we took advantage of three specific inhibitors, including SP600125, a pan-JNK inhibitor; SB203580, a p38 inhibitor; and U0216, a MEK inhibitor. Although none of these three inhibitors at various doses was able to rescue the G2/M arrest in HK-2 cells treated with aristolochic acid, R03306 or paclitaxel (Fig. 6b and data not shown), SP600125 decreased the upregulation of mRNA levels of profibrogenic genes induced by aristolochic acid, R03306 or paclitaxel by ∼40–80% (Fig. 6b). The MEK inhibitor, by contrast, exacerbated the increase in profibrogenic gene upregulation (amplified by an extra fivefold), whereas the p38 inhibitor did not affect the gene activation in these conditions (data not shown). The secretion of CTGF by HK-2 cells treated with aristolochic acid, RO3306 or paclitaxel was decreased by ∼75% in the presence of the JNK inhibitor (shown with aristolochic acid in Fig. 6c). In addition, the increased proliferation and collagen production in fibroblasts triggered by conditioned medium from aristolochic acid–treated HK-2 cells were diminished by ∼80% and ∼60%, respectively when we also treated aristolochic acid–treated HK-2 cells with the JNK inhibitor (Fig. 6d,e). Examination of kidney sections from the fibrotic AKI models revealed colocalization of JNK signaling activation markers (p-JNK and p–c-jun immunoreactivity) with p-H3–positive nuclei in all injury models (shown for the AAN model in Fig. 6f). To test the role of JNK in the fibrotic response *in vivo*, we injected mice intraperitoneally with SP600125 (1 mg per day), starting at 7 d after unilateral IRI, after the acute injury phase was over, and continued the treatment until 28 d after surgery. We introduced the treatment at 7 d to avoid potential effects of the drug on the degree of acute injury, inflammation, cell proliferation and the onset of epithelial G2/M arrest in the unilateral IRI model (Fig. 2). JNK inhibition *in vivo* reduced fibrosis (Fig. 6g,h), kidney collagen content (Fig. 6h) and mRNA levels of *Tgfb1*, *Ctgf*, *Col4a1* and *Col1a1* in the unilateral IRI model (Fig. 6i).

## Discussion

Fibrosis is a common event that leads to the derangement of tissue structure and irreversible loss of normal organ function. In the kidney, tubulointerstitial fibrosis is a poor prognostic indicator and represents a common final pathway in the progression to end-stage renal disease, irrespective of the initial cause. Acute kidney injury has been recognized as a major contributor to chronic and end-stage kidney disease[33]. A fundamental unanswered question in understanding the pathogenesis of kidney fibrosis is the nature of the molecular switch that differentiates renal tubular reparative from fibrotic responses to injury. Our results indicate that proximal tubular cells arrested in the G2/M stage of the cell cycle after injury produce profibrogenic growth factors that are capable of stimulating fibroblast proliferation and collagen production.

Here we characterized the time-dependent cell cycle progression *in vivo* in five models of acute kidney injury in the mouse. Through this analysis, we found a strong correlation between G2/M arrest in tubular cells and a fibrotic outcome. The profibrotic effects were

greatly attenuated when we reduced the time spent in G2/M *in vitro* and *in vivo*, either by inhibition of the ATM pathway or by contralateral nephrectomy, another maneuver that facilitates movement out of the G2/M phase of the cell cycle.

Cell cycle analysis *in vivo* proved to be a predictive tool for determining the progression of kidney injury to either normal proximal tubule cell proliferation and epithelial repair or fibrosis. The ability to identify cell types, including nephron segment or nontubular cells, and cell cycle stage all resolved in time, provides the opportunity to study repair processes at cellular resolution. These observations identified the tubular cells as crucial participants in the fibrotic fate. The association *in vitro* and *in vivo* of G2/M arrest and production of profibrogenic growth factors from the tubular cells under a number of conditions where G2/M is altered independently provides additional evidence that tubular cells arrested in G2/M have a primary role in determining the fibrotic response.

The major factors investigated here and shown to be upregulated in the G2/M-arrested tubular cells were TGF-β1 and CTGF. TGF-β1 is a well-established principal driver of fibrosis via promotion of fibroblast proliferation, extracellular matrix synthesis and inhibition of collagenases in multiple organs[34,35]. CTGF is a key downstream effector of profibrotic TGF-β1 activity. CTGF acts both in TGF-β1–independent and TGF-β1–dependent fashions and has proved to have key roles in the development of fibrosis in multiple organs, including the kidney[36–39].

There are a number of previous studies where findings can be re-interpreted as supportive of conclusions that proximal tubule G2/M arrest leads to fibrosis. Interpretations of cellular senescence and active cell cycle kinetics have focused previous analyses on cell cycle regulation at the restriction point that permits transition from G1 to S. These same regulators (for example, p53, p21 and p19INK) can all act during G2 to prevent mitotic progression after genotoxic stress[41]. For example, p53 has a key role at the G2 checkpoint that regulates the G2/M transition in response to stress and DNA damage[41]. p21 is a transcriptional target of p53 and also participates in the G2 checkpoint by inhibiting cyclin-dependent kinases[42]. *Trp53* deficiency results in less kidney interstitial fibrosis in unilateral IRI mice[43]. Mice lacking the p21 gene product have a greater hyperplastic response and do not develop renal dysfunction or interstitial fibrosis after partial renal ablation. This protection may be related to a reduced amount of cell cycle arrest than that seen in normal mice with intact p21 (ref. 44). Evidence for other G2/M arrest models comes from mice null for *Stmn*, encoding stathmin, which regulates the G2/M transition by being necessary for the proper formation of the mitotic spindle. These mice show delayed recovery, prolonged tubular proliferation and interstitial fibrosis after ischemic-reperfusion injury[45]. It is possible that normal nonfibrotic repair depends on efficient dedifferentiation of the surviving epithelial cells, which is dependent upon reduced p53-p21 pathway activation. If this pathway is activated, G2/M arrest occurs, reducing the efficiency of normal repair. It has recently been shown that the p53-p21 pathway is activated during the reprogramming of somatic cells to induced pluripotent stem cells, and inhibition of this pathway markedly improves dedifferentiation and greatly facilitates proliferation of the cells[46–48].

In conclusion, the unique cell cycle data set from our current study, supported by our observations with PIF-α and contralateral nephrectomy after unilateral ischemia, indicate that G2/M arrest in proximal tubule cells after kidney injury results in abnormal amplification of profibrogenic factors. This serves as a mechanistic link between AKI and chronic progressive fibrotic kidney disease. Our data indicate that JNK, known to enhance TGF-β1 and CTGF gene transcription and promote fibrosis[49], is activated during G2/M arrest and upregulates profibrotic gene expression *in vitro* and collagen production *in vivo*, whereas inhibition of JNK activity protects the kidney against the development of fibrosis.

Maintaining the proper progression of tubular epithelial cells through the cell cycle during the injury phase is a potential therapeutic goal to prevent interstitial fibrosis and accelerated progression of chronic kidney disease.

## Online Methods

### Induction of acute kidney injury in mice

Male BALB/c mice aged 8 to 10 weeks weighing 20–22 g were purchased from Charles River Laboratories. All mouse work was performed in accordance with the animal use protocol approved by the Institutional Animal Care and User Committee of the Harvard Medical School.

Ischemia was induced by the retroperitoneal approach on both kidneys for 30 min at 37.0 °C (moderate IRI) or for 32 min at 37.5 °C (severe IRI) or only the left kidney for 30 min at 37 °C (unilateral IRI), as previously reported[50]. One milliliter of warm saline (37 °C) was injected intraperitoneally after surgery for volume supplement. Sham operations were performed with exposure of both kidneys but without induction of ischemia. The UUO model was generated by ligation of the left ureter. Acute aristolochic acid nephropathy was induced by a one-time intraperitoneal injection of aristolochic acid (5 mg per kg body weight, Sigma) in PBS. The normal control mice were administered the same amount of PBS. For the moderate IRI-paclitaxel model, moderate bilateral IRI was induced, and then the mice were injected intraperitoneally with paclitaxel (Sigma, 20 mg per kg body weight with 0.1% DMSO in PBS) on days 1 and 4 after the surgery. In controls, 0.1% DMSO in PBS was administered to the moderate IRI group. For the rescue of fibrosis in the unilateral IRI model, three approaches were taken in several groups of mice: nephrectomy of contralateral kidney was performed 3 d after unilateral IRI surgery, mice were given PIF-α (Sigma, 2.2 mg per kg body weight) intraperitoneally on days 3 and 14 after surgery or mice were injected with SP600125 (Sigma, 1 mg per day), started 7 d after surgery. PBS (PIF-α solvent) or DMSO (SP600125 solvent) was injected in the control groups. In each mouse group in which cell cycle analysis was performed, all mice received an intraperitoneal injection of BrdU (10 mg $ml^{-1}$ in PBS, 100 mg per kg body weight) 2 h prior to killing. In other mice, BrdU was injected 12 h, 8 h or 4 h before killing.

### Renal function and histology

The plasma creatinine concentration was determined by the picric acid method[45]. Kidney histology was examined on formalin sections stained with H&E and Masson's trichrome. The degree of interstitial fibrosis was scored semiquantitatively on a 0 to 4 scale (0, no lesion; 1, <25% of parenchyma affected by the lesion; 2, >25–50% of parenchyma affected by the lesion; 3, >50–75% of parenchyma affected by the lesion; 4, >75% of parenchyma affected by the lesion). The collagen content of kidneys was quantified with the Sircol soluble collagen assay kit (Biocolor).

### Isolation of tubules from kidney

The kidney cortex was dissected, diced and digested in DMEM containing Liberase CI (40 μg $ml^{-1}$, Roche) with a gentleMACS dissociator (Miltinyi Biotech). The enzyme reaction was terminated with horse serum (Gibco) at 4 °C, and then the tubule suspension was passed through 40-μm and 70-μm cell meshes (BD Falcon) sequentially. Tubules were collected with cold PBS from the 70-μm mesh and protein, and RNA was extracted immediately.

### Cell culture and treatment

The HK-2 (human), LLC-PK1 (pig) and IRPTC (rat) proximal cell lines and NIH 3T3 fibroblast cell line (American Type Culture Collection) were cultured in DMEM medium

supplemented with 10% FCS until the cells were 80% confluent. Cells were then incubated in DMEM medium containing 0.2% FCS for 24 h and treated with either aristolochic acid (5 μg $ml^{-1}$), aristolochic acid with KU55933 (Sigma, 1 μM) or aristolochic acid with SP600125 or SB203580 or U0216 (Sigma, 10 μM). RO3306 (Sigma, 9 μM) or paclitaxel (50 nM to 10 μM) were added to normal growing cells maintained in 5–10% FCS medium. In some experiments, after 48 h treatment of HK-2 cells with aristolochic acid, the drug was washed out and the cells continued in culture for 24 h. The conditioned medium was then collected and added to serum-starved NIH 3T3 fibroblasts. Experiments had been done confirming that when aristolochic acid was washed out for 24 h, the HK-2 cells were still arrested in G2/M and maintained high levels of TGF-β1 and CTGF production (data not shown).

### RNA interference–mediated knockdown of ATM

Short hairpin RNA lentiviral plasmids (pLKO.1) targeting ATM were purchased from Sigma. The shATM sequences used were as follows: 5′-TGATGGTCTTAAGGAACATCT-3′ (catalog no. TRCN0000010299) and 5′-CCTTTCATTCAGCCTTTAGAA-3′ (catalog no. TRCN0000194861) for HK-2 cells and 5′-GGCCTCCAATTCTTCACAGTA-3′ (catalog no. TRCN0000039951) for LLC-PK1 cells. The pLKO.1-shGFP directed against GFP, target 5′-GCAAGCTGACCCTGAAGTTCA-3′, was purchased from Addgene. Virus titers were adjusted for maximal knockdown of ATM.

### Fluorescence-activated cell sorting analysis for cell cycle distribution

Cells were prepared for propidium iodide (Sigma) staining according to standard protocols. DNA content was determined with a FACSCaliber (Becton Dickinson FACScan) Analyzer. Hoechst 33324 (Sigma, 10 μM) was used to stain the live HK-2 cells, and, through ultraviolet-MoFlo sorting (DakoCytomation High Speed MoFlo Sorter), cells in G0/G1 or G2/M phase were isolated, and RNA and protein were extracted immediately afterward.

### Quantification of mRNA by real-time quantitative reverse transcription PCR and transforming growth factor-β1 protein determination

Total RNA was isolated from either the kidneys or the cultured tubular cells with TRIzol reagent (Sigma) according to the standard protocol. Five micrograms of total RNA was reverse transcribed with the M-MLV reverse transcriptase Kit and Oligo dT primers (Promega). Real-time PCR was performed by TaqMan gene expression assays (Applied Biosystems) for detection of mRNA expression of *TGFB1*, *CTGF*, *COL4A11*, *COLA11* and *ACTA2*. *GAPDH* was the internal control. TGF-β1 protein concentration was assayed by the commercial ELISA kit (R&D).

### Western blot analysis

Cells or kidney tissues were lysed, and lysates were prepared as previously described[51]. Membranes were incubated with one or more of the following primary antibodies: mouse antibody to ATM and antibody to p53 (Santa Cruz, 1 in 500), mouse antibody to p-ATM (Ser1981) and rabbit antibody to Chk2, p-Chk2 (Ser68), p-p53 (Ser15), JNK, p-JNK, c-jun, p–c-jun, p38, p-p38, ERK and p-ERK (Cell Signaling, 1 in 1,000); and rabbit antibody to collagen IV (Abcam, 1 in 5,000). Horseradish peroxidase–conjugated secondary antibodies were applied, and enhanced chemiluminescence (Amersham Biosciences) was used to detect proteins. β-actin–specific (Sigma) antibody was used for loading controls on stripped membranes. Supernatant from cultured HK-2 cells was tested for CTGF protein abundance with rabbit CTGF–specific antibody (Abcam, 1 in 5,000).

### Immunofluorescence staining

Immunofluorescence staining of the kidney was performed on paraffin sections as previously described[52]. Briefly, the tissue sections were rehydrated and labeled with antibodies, including rabbit antibody to Ki-67 (Vector, 1 in 200), mouse antibody to BrdU (Becton Dickinson, 1 in 100), mouse antibody to p-H3 (Ser10) (Abcam, 1 in 10,000), FITC-coupled peanut lectin (Sigma, 1 in 500), rabbit antibody to Kim-1 (R9 (ref. 24), 1 in 200), mouse antibody to p-ATM Ser1981 (Active Motif, 1 in 500), mouse antibody to p-ATR (Ser428) (Cell Signaling, 1 in 200), rabbit antibody to α-SMA (Sigma, 1 in 400), rabbit antibodies to p-H3 (Ser10), TGF-β1 and CTGF (Santa Cruz, 1 in 200), rabbit antibody to collagen IV (Abcam, 1 in 500) and rabbit antibody to phospho-JNK and p–c-jun (Cell Signaling, 1 in 500 and 1 in 200). The slides were then exposed to FITC or Cy3-labeled secondary antibodies (Jackson ImmunoResearch). The staining was examined with fluorescence microscopes (Nikon TE 1000 and Nikon C1 confocal). Immunofluorescence staining of p-ATM (Ser1981) was also performed on HK-2 cells as previously described[52].

### Cell death assay

Apoptosis in kidney tissues was detected on paraffin sections by *in situ* TUNEL method following the standard protocol (Roche). Apoptosis in HK-2 cells was determined with a MEBCYTO Apoptosis Kit (MBL). Cells were incubated with a mixture of annexin V–FITC and propidium iodide, and apoptosis was measured by flow cytometry.

### Statistical analyses

Analysis of variance was used to compare data among groups. Student's *t* test was used to determine a significant difference between two groups. A $P$ value of less than 0.05 was considered significant. The results are presented as means ± s.d.

## Supplementary Material

Refer to Web version on PubMed Central for supplementary material.

## Acknowledgments

This work was supported by US National Institutes of Health (NIH) grants DK39773 and DK72381 to J.V.B. and DK074030 to J.V.S. L.Y. was supported by a fellowship from the International Society of Nephrology.

## References

1. Humphreys BD, et al. Intrinsic epithelial cells repair the kidney after injury. Cell Stem Cell. 2008; 2:284–291. [PubMed: 18371453]
2. Wynn TA. Cellular and molecular mechanisms of fibrosis. J Pathol. 2008; 214:199–210. [PubMed: 18161745]
3. Coresh J, Astor BC, Greene T, Eknoyan G, Levey AS. Prevalence of chronic kidney disease and decreased kidney function in the adult US population: Third National Health and Nutrition Examination Survey. Am J Kidney Dis. 2003; 41:1–12. [PubMed: 12500213]
4. Lameire N, Jager K, Van Biesen W, de Bacquer D, Vanholder R. Chronic kidney disease: a European perspective. Kidney Int Suppl. 2005:S30–S38. [PubMed: 16336574]
5. Forbes JM, Hewitson TD, Becker GJ, Jones CL. Ischemic acute renal failure: long-term histology of cell and matrix changes in the rat. Kidney Int. 2000; 57:2375–2385. [PubMed: 10844607]
6. Macedo E, Bouchard J, Mehta RL. Renal recovery following acute kidney injury. Curr Opin Crit Care. 2008; 14:660–665. [PubMed: 19005306]
7. Kalluri R, Neilson EG. Epithelial-mesenchymal transition and its implications for fibrosis. J Clin Invest. 2003; 112:1776–1784. [PubMed: 14679171]

8. Liu Y. Epithelial to mesenchymal transition in renal fibrogenesis: pathologic significance, molecular mechanism, and therapeutic intervention. J Am Soc Nephrol. 2004; 15:1–12. [PubMed: 14694152]
9. Burns WC, Kantharidis P, Thomas MC. The role of tubular epithelial-mesenchymal transition in progressive kidney disease. Cells Tissues Organs. 2007; 185:222–231. [PubMed: 17587828]
10. Humphreys BD, et al. Fate tracing reveals the pericyte and not epithelial origin of myofibroblasts in kidney fibrosis. Am J Pathol. 2010; 176:85–97. [PubMed: 20008127]
11. Nguyen TQ, Goldschmeding R. Bone morphogenetic protein-7 and connective tissue growth factor: novel targets for treatment of renal fibrosis? Pharm Res. 2008; 25:2416–2426. [PubMed: 18266088]
12. Qi W, Chen X, Poronnik P, Pollock CA. Transforming growth factor-β/connective tissue growth factor axis in the kidney. Int J Biochem Cell Biol. 2008; 40:9–13. [PubMed: 17300978]
13. Bonventre JV. Dedifferentiation and proliferation of surviving epithelial cells in acute renal failure. J Am Soc Nephrol. 2003; 14(1):S55–S61. [PubMed: 12761240]
14. Price PM, Megyesi J, Safirstein RL. Cell cycle regulation: repair and regeneration in acute renal failure. Kidney Int. 2004; 66:509–514. [PubMed: 15253699]
15. Tanaka H, et al. Role of the E2F1-p19-p53 pathway in ischemic acute renal failure. Nephron Physiol. 2005; 101:27–34.
16. Chkhotua AB, Abendroth D, Froeba G, Schelzig H. Up-regulation of cell cycle regulatory genes after renal ischemia/reperfusion: differential expression of p16(INK4a), p21(WAF1/CIP1) and p27(Kip1) cyclin-dependent kinase inhibitor genes depending on reperfusion time. Transpl Int. 2006; 19:72–77. [PubMed: 16359379]
17. Melk A, Schmidt BM, Vongwiwatana A, Rayner DC, Halloran PF. Increased expression of senescence-associated cell cycle inhibitor p16INK4a in deteriorating renal transplants and diseased native kidney. Am J Transplant. 2005; 5:1375–1382. [PubMed: 15888044]
18. Jiang M, Dong Z. Regulation and pathological role of p53 in cisplatin nephrotoxicity. J Pharmacol Exp Ther. 2008; 327:300–307. [PubMed: 18682572]
19. Price PM, Safrstein RL, Megyesi J. The cell cycle and acute kidney injury. Kidney Int. 2009; 76:604–613. [PubMed: 19536080]
20. Molitoris BA, et al. siRNA targeted to p53 attenuates ischemic and cisplatin-induced acute kidney injury. J Am Soc Nephrol. 2009; 20:1754–1764. [PubMed: 19470675]
21. Yu CC, Woods AL, Levison DA. The assessment of cellular proliferation by immunohistochemistry: a review of currently available methods and their applications. Histochem J. 1992; 24:121–131. [PubMed: 1349881]
22. Crosio C, et al. Mitotic phosphorylation of histone H3: spatio-temporal regulation by mammalian Aurora kinases. Mol Cell Biol. 2002; 22:874–885. [PubMed: 11784863]
23. Silva FG, Nadasdy T, Laszik Z. Immunohistochemical and lectin dissection of the human nephron in health and disease. Arch Pathol Lab Med. 1993; 117:1233–1239. [PubMed: 8250694]
24. Ichimura T, Hung CC, Yang SA, Stevens JL, Bonventre JV. Kidney injury molecule-1: a tissue and urinary biomarker for nephrotoxicant-induced renal injury. Am J Physiol Renal Physiol. 2004; 286:F552–F563. [PubMed: 14600030]
25. Hendzel MJ, et al. Mitosis-specific phosphorylation of histone H3 initiates primarily within pericentromeric heterochromatin during G2 and spreads in an ordered fashion coincident with mitotic chromosome condensation. Chromosoma. 1997; 106:348–360. [PubMed: 9362543]
26. Abraham RT. Cell cycle checkpoint signaling through the ATM and ATR kinases. Genes Dev. 2001; 15:2177–2196. [PubMed: 11544175]
27. Goodarzi AA, Block WD, Lees-Miller SP. The role of ATM and ATR in DNA damage-induced cell cycle control. Prog Cell Cycle Res. 2003; 5:393–411. [PubMed: 14593734]
28. Bencokova Z, et al. ATM activation and signaling under hypoxic conditions. Mol Cell Biol. 2009; 29:526–537. [PubMed: 18981219]
29. Hickson I, et al. Identification and characterization of a novel and specific inhibitor of the ataxia-telangiectasia mutated kinase ATM. Cancer Res. 2004; 64:9152–9159. [PubMed: 15604286]
30. Komarov PG, et al. A chemical inhibitor of p53 that protects mice from the side effects of cancer therapy. Science. 1999; 285:1733–1737. [PubMed: 10481009]

31. Vassilev LT, et al. Selective small-molecule inhibitor reveals critical mitotic functions of human CDK1. Proc Natl Acad Sci USA. 2006; 103:10660–10665. [PubMed: 16818887]
32. Horwitz SB. Mechanism of action of taxol. Trends Pharmacol Sci. 1992; 13:134–136. [PubMed: 1350385]
33. Ishani A, et al. Acute kidney injury increases risk of ESRD among elderly. J Am Soc Nephrol. 2009; 20:223–228. [PubMed: 19020007]
34. Leask A, Abraham DJ. TGF-β signaling and the fibrotic response. FASEB J. 2004; 18:816–827. [PubMed: 15117886]
35. Zeisberg M, et al. Fibroblasts derive from hepatocytes in liver fibrosis via epithelial to mesenchymal transition. J Biol Chem. 2007; 282:23337–23347. [PubMed: 17562716]
36. Qi W, et al. Integrated actions of transforming growth factor-β1 and connective tissue growth factor in renal fibrosis. Am J Physiol Renal Physiol. 2005; 288:F800–F809. [PubMed: 15536170]
37. Okada H, et al. Connective tissue growth factor expressed in tubular epithelium has a pivotal role in renal fibrogenesis. J Am Soc Nephrol. 2005; 16:133–143. [PubMed: 15574513]
38. Ikawa Y, et al. Neutralizing monoclonal antibody to human connective tissue growth factor ameliorates transforming growth factor-β–induced mouse fibrosis. J Cell Physiol. 2008; 216:680–687. [PubMed: 18481257]
39. Shi-Wen X, Leask A, Abraham D. Regulation and function of connective tissue growth factor/CCN2 in tissue repair, scarring and fibrosis. Cytokine Growth Factor Rev. 2008; 19:133–144. [PubMed: 18358427]
40. Stark GR, Taylor WR. Control of the G2/M transition. Mol Biotechnol. 2006; 32:227–248. [PubMed: 16632889]
41. Taylor WR, Stark GR. Regulation of the G2/M transition by p53. Oncogene. 2001; 20:1803–1815. [PubMed: 11313928]
42. Bunz F, et al. Requirement for p53 and p21 to sustain G2 arrest after DNA damage. Science. 1998; 282:1497–1501. [PubMed: 9822382]
43. Kailong L, et al. P53-Rb signaling pathway is involved in tubular cell senescence in renal ischemia/reperfusion injury. Biocell. 2007; 31:213–223. [PubMed: 17902269]
44. Megyesi J, Price PM, Tamayo E, Safirstein RL. The lack of a functional p21(WAF1/CIP1) gene ameliorates progression to chronic renal failure. Proc Natl Acad Sci USA. 1999; 96:10830–10835. [PubMed: 10485911]
45. Zahedi K, et al. Stathmin-deficient mice develop fibrosis and show delayed recovery from ischemic-reperfusion injury. Am J Physiol Renal Physiol. 2006; 290:F1559–F1567. [PubMed: 16434570]
46. Hong H, et al. Suppression of induced pluripotent stem cell generation by the p53-p21 pathway. Nature. 2009; 460:1132–1135. [PubMed: 19668191]
47. Kawamura T, et al. Linking the p53 tumour suppressor pathway to somatic cell reprogramming. Nature. 2009; 460:1140–1144. [PubMed: 19668186]
48. Marion RM, et al. A p53-mediated DNA damage response limits reprogramming to ensure iPS cell genomic integrity. Nature. 2009; 460:1149–1153. [PubMed: 19668189]
49. Ma FY, Sachchithananthan M, Flanc RS, Nikolic-Paterson DJ. Mitogen activated protein kinases in renal fibrosis. Front Biosci (Schol Ed). 2009; 1:171–187. [PubMed: 19482693]
50. Park KM, et al. Inducible nitric oxide synthase is an important contributor to prolonged protective effects of ischemic preconditioning in the mouse kidney. J Biol Chem. 2003; 278:27256–27266. [PubMed: 12682064]
51. Hung CC, Ichimura T, Stevens JL, Bonventre JV. Protection of renal epithelial cells against oxidative injury by endoplasmic reticulum stress preconditioning is mediated by ERK1/2 activation. J Biol Chem. 2003; 278:29317–29326. [PubMed: 12738790]
52. Ichimura T, et al. Kidney injury molecule-1 is a phosphatidylserine receptor that confers a phagocytic phenotype on epithelial cells. J Clin Invest. 2008; 118:1657–1668. [PubMed: 18414680]

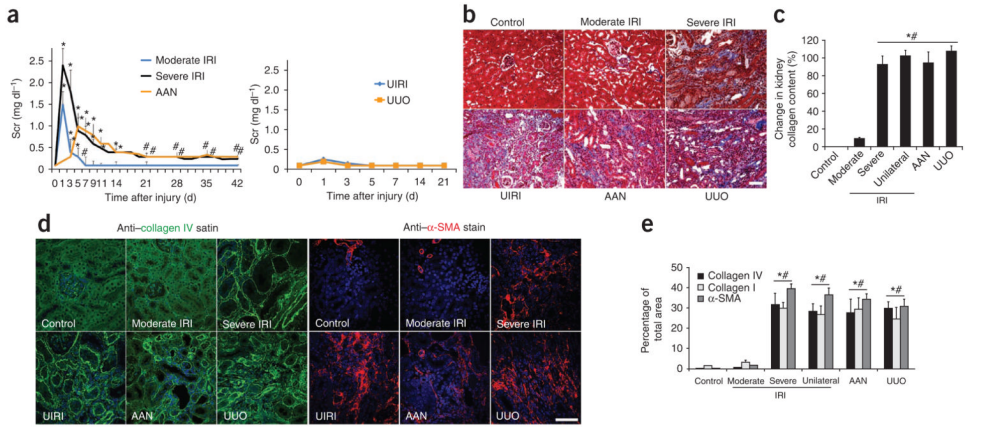


**Figure 1.**

Clinical-pathological features of AKI models. (**a**) Changes of serum creatinine over time in AKI mouse models, including moderate and severe IRI and AAN (left) and unilateral IRI (UIRI) and UUO (right) models ($n = 8$ for each time point). $^{*}P < 0.001$, $^{\#}P < 0.01$ versus day 0 before procedure. (**b**) Histology of the fibrotic outcomes of the AKI models ($n = 3$ mice in each group, Masson's trichrome staining showing fibrosis with blue color). (**c**) Sircol assay of kidney collagen content in the five AKI models ($n = 3$ mice in each group). $^{*}P < 0.001$ versus control, $^{\#}P < 0.001$ versus moderate IRI. (**d**) Immunostaining of collagen IV (left, green (anti–collagen IV)) and α-SMA (right, red (anti–α-SMA)) in AKI models ($n = 3$ mice in each group). (**e**) The percentage of total tissue area that stained positively for collagen IV, collagen I and α-SMA in the kidneys at 42 d (moderate IRI, severe IRI, UIRI and AAN) or 14 d (UUO). $^{*}P < 0.001$ versus control, $^{\#}P < 0.001$ versus moderate IRI. Scale bars, 50 μm. Error bars represent s.d.

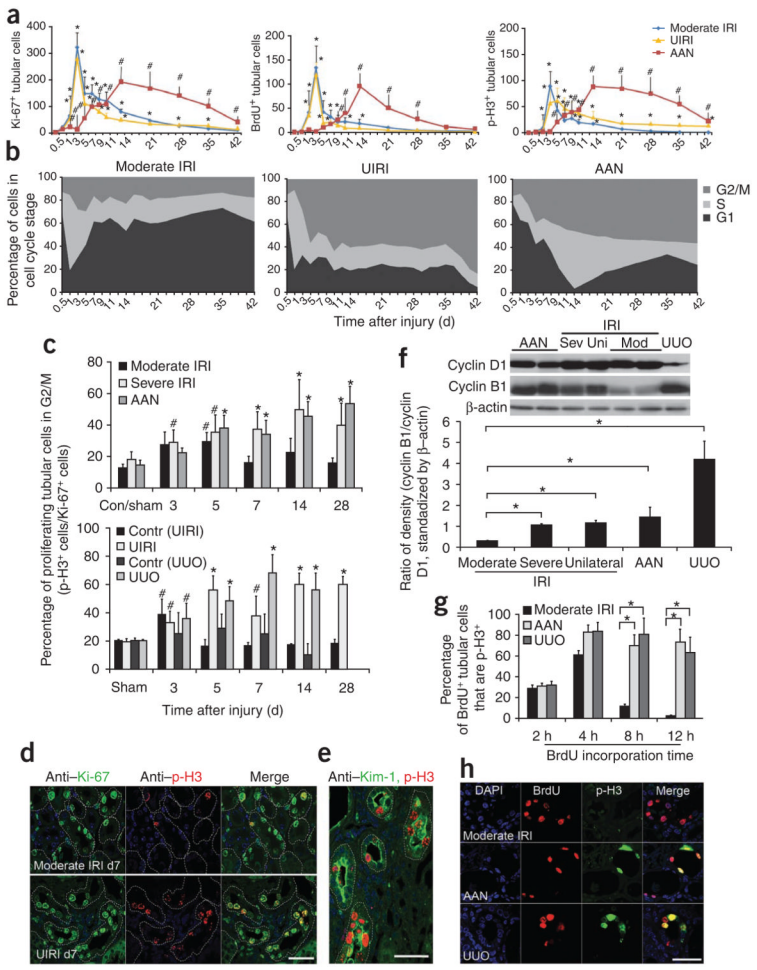


**Figure 2.**

Repair of renal tubular cells in models of AKI. (**a**) Number (per 400× field) of Ki-67–positive (left), BrdU-positive (middle) or p-H3–positive (right) tubular cells in moderate IRI, UIRI and AAN mice ($n = 3$ mice at each time point in each group). *$P < 0.01$ versus sham, $^{\#}P < 0.01$ versus control. (**b**) Cell cycle distribution (G1, S and G2/M) of tubular cells in moderate IRI (left), UIRI (middle) and AAN (right) models as a function of time after the insult ($n = 3$ mice of each time point in each group). (**c**) Percentage of the proliferating (Ki-67–positive) tubular cells that are in the G2/M phase of the cell cycle in the AKI models in moderate IRI, UIRI and AAN (top) and UIRI and UUO models (bottom), showing both the injured kidney and the contralateral kidney (contr). *$P < 0.001$, $^{\#}P < 0.01$ versus control or sham ($n = 3$ mice of each time point in each group). (**d**) Coimmunostaining with antibodies to Ki-67 (anti–Ki-67) and p-H3 (anti–p-H3) on day-7 kidneys from the moderate and UIRI groups. (**e**) Coimmunostaining with antibodies to p-H3 and Kim-1 (anti–Kim-1) in UIRI mice. The tubular basement membrane is outlined. (**f**) Western blot analysis of cyclin D1 and cyclin B1 in isolated tubules from AKI kidneys (top) and ratio of cyclin B1 to cyclin D1 densities standardized to β-actin (bottom). *$P < 0.001$. (**g**) Percentage of BrdU-positive tubular cells that are in G2/M at various times after BrdU administration in the moderate IRI, AAN and UUO groups. *$P < 0.001$. (**h**) Staining with antibodies to BrdU and p-H3, as well as of nuclei with DAPI, in moderate IRI, AAN and UUO mice that were injected with BrdU at 12 h before killing. Scale bars, 50 μm. Error bars represent s.d.

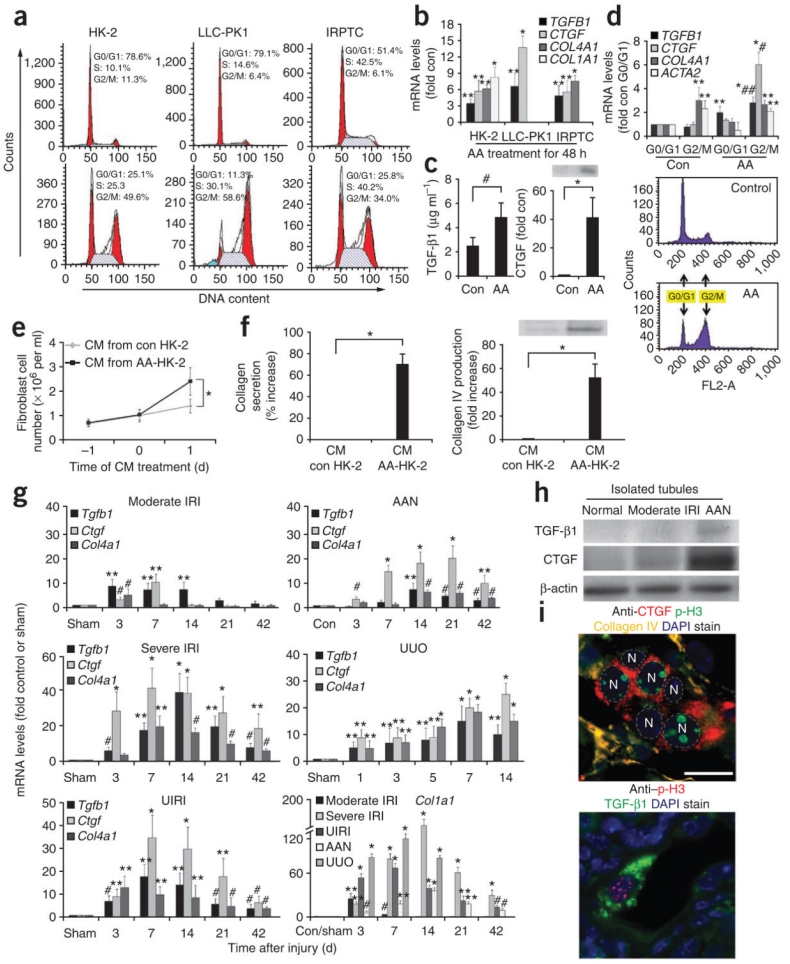


**Figure 3.**

Profibrogenic factor production in G2/M-arrested proximal tubular cells *in vitro* and in AKI models *in vivo*. (**a**) Cell cycle analysis by propidium iodide staining and flow cytometry in HK-2, LLC-PK1 or IRPTC cells at baseline (top three graphs) and after treatment with aristolochic acid at 5 μg ml$^{-1}$ for 48 h (bottom three graphs). ($n$ = 10, $n$ = 3 and $n$ = 3 experiments for the three cell types, respectively.) (**b**) Quantification of mRNA levels of profibrogenic genes in HK-2, LLC-PK1 and IRPTC cells treated with aristolochic acid (AA) at 5 μg ml$^{-1}$ for 48 h, expressed as fold increases over controls ($n$ = 6, $n$ = 3 and $n$ = 3 experiments). *$P$ < 0.001, **$P$ < 0.01 versus control. (**c**) TGF-β1 concentration (left) and fold increase in CTGF protein concentrations (right) in the supernatant of HK-2 cells treated with aristolochic acid for 48 h. *$P$ < 0.001, $^{\#}P$ < 0.05. (**d**) Changes in mRNA levels of profibrogenic factors in cells in various cell cycle phases with or without previous aristolochic acid treatment ($n$ = 6). *$P$ < 0.01, **$P$ < 0.05 versus control G0/G1; $^{\#}P$ < 0.01, $^{\#\#}P$ < 0.05 versus control G2/M. (**e**) Effect of conditioned medium from G2/M-arrested HK-2 cells on cell proliferation of serum-starved fibroblasts. *$P$ < 0.05. ($n$ = 3.) (**f**) Collagen secretion (left) and collagen IV production (right) in fibroblasts treated with conditioned medium from control or G2/M-arrested HK-2 cells, presented as percentage increase (collogen) or fold increase (collagen IV) in response to CM from AA-treated HK-2 cells versus CM from untreated HK-2 cells. ($n$ = 3.) *$P$ < 0.01. (**g**) mRNA levels of profibrogenic factors as a function of time in AKI models, including moderate IRI, severe IRI, UIRI, AAN and UUO ($n$ = 3 mice per time point in each group). *$P$ < 0.001, **$P$ <

0.01, $^{\#}P < 0.05$ versus control or sham (set arbitrarily to 1). (**h**) Western blot analysis of TGF-β1 and CTGF in isolated tubules from moderate IRI and aristolochic acid–treated mice. (**i**) Co-staining of CTGF or TGF-β1 with p-H3. Nuclei (N) are outlined in the top image. Scale bar, 10 μm. Error bars represent s.d.

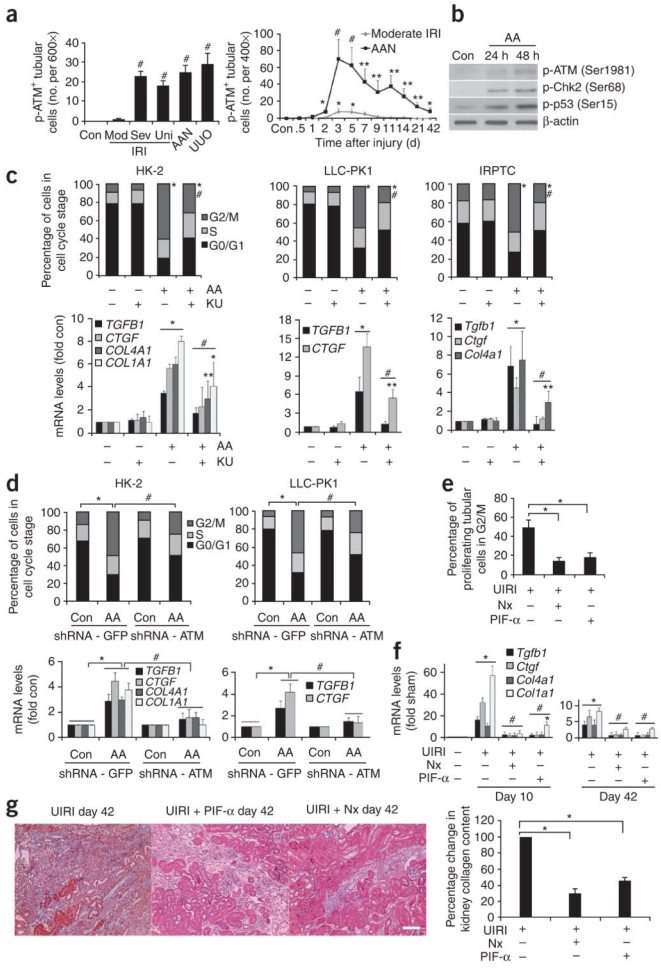


**Figure 4.**

Reversal of G2/M arrest rescues the fibrogenic effect in aristolochic acid-treated HK-2 cells and in the UIRI mouse model. (**a**) Number of proximal tubule cells per 600× fieldthat were positive for p-ATM (Ser1981) for all ofthe models on day 3 (left) and a temporal curve of p-ATM–positive cells in a 400× field for the moderate IRI and AAN insults (right, $n = 3$ mice per time point in each group). $^{*}P < 0.05$, $^{**}P < 0.01$, $^{\#}P < 0.001$ versus control or sham. (**b**) Western blot analysis of p-ATM, p-Chk2 (Ser68) and p-p53 (Ser15) in HK-2 cells treated with aristolochic acid (AA). (**c**) Effects of KU 55933 (an ATM inhibitor) on cell cycle changes (top) and profibrogenic gene expression (bottom) in HK-2cells (left), LLC-PK1 cells (middle) and IRPTC cells (right) treated with AA for 48 h ($n = 3$). $^{*}P < 0.01$,$^{**}P < 0.05$ versus control; $^{\#}P < 0.05$ versus AA. (**d**) Cell cycle distribution (top) and profibrogenic factor production (bottom) in HK-2 cells and LLC-PK1 cells with or without previous ATM shRNA treatment. ($n = 3$.) $^{*}P < 0.01$, $^{\#}P < 0.05$. Symbols in the cell cycle data panels refer to the comparison of G2/M phases. (**e**) Percentage of proliferating tubular cells in G2/M in kidneys from UIRI mice and UIRI mice that had undergone contralateral nephrectomy (N) or PIF-α treatment 10 d after the UIRI. $^{*}P < 0.01$. (**f**) The mRNA levels of whole-kidney *Tgfb1*, *Ctgf*, *Col4a1* and *Col1a1* in UIRI mice with contralateral Nx or PIF-α treatment. $^{*}P < 0.01$, versus sham; $^{\#}P < 0.05$ versus UIRI. (**g**) The effect of Nx or PIF-α treatment on the degree of interstitial fibrosis in the UIRI kidneys (examined 42 d after UIRI injury), as indicated by staining with Masson's trichrome (left) and collagen content determined with

the Sircol assay (right). Scale bar, 50 μm. *$P < 0.01$. Error bars represent s.d. For the mRNA levels in **c** and **d**, the control values were orbitrarily set to 1.

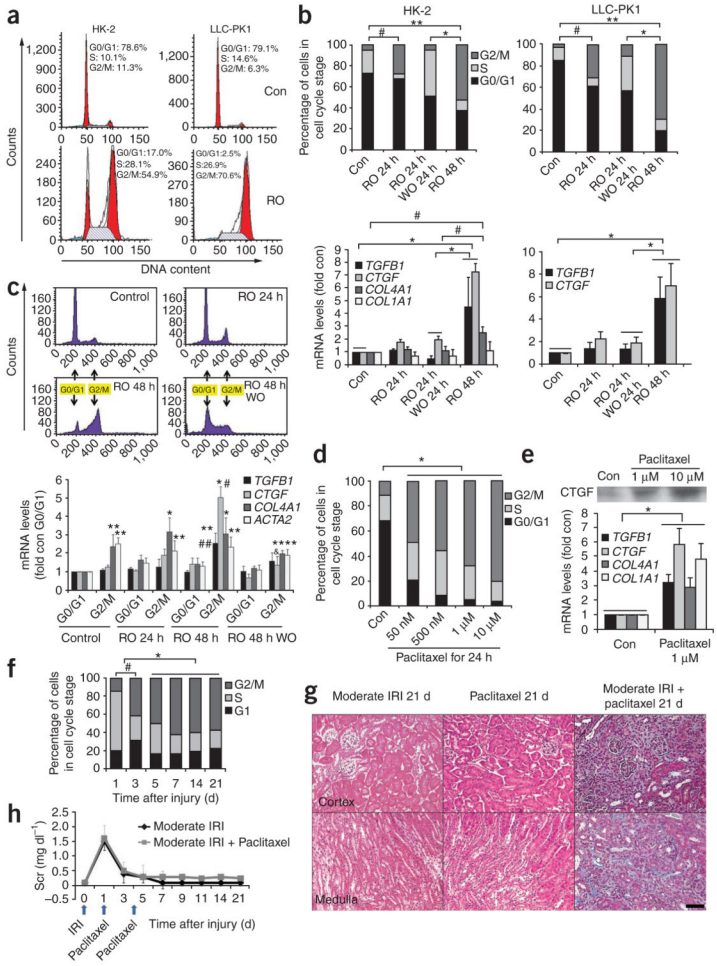


**Figure 5.**

Prolonged G2/M arrest, induced by alternative strategies, causes a profibrotic phenotype both *in vitro* and *in vivo*. (**a**) Cell cycle changes in HK-2 and LLC-PK1 cells treated with RO3306 (RO) for 48 h. (**b**) Cell cycle changes (top) and profibrotic gene expression (bottom) in HK-2 and LLC-PK1 cells treated with RO3306 for 24 h (RO24 h) or 48 h (RO 48 h). ($n$ = 3.) In one group, the RO3306 drug was washed out after 24 h and the cells examined 24 h later (RO 24 h/WO 24 h). $^{**}P < 0.001$, $^{*}P < 0.01$, $^{\#}P < 0.05$. (**c**) Cell cycle distribution of normal cycling HK-2 cells (control), cells treated with RO3306 for 24 h (RO 24 h), cells treated with RO3306 for 48 h (RO 48 h) and cells treated with RO3306 for 48 h and then collected 6 h after washout of the RO3306 (RO 48 h WO) (top) and mRNA levels of profibrogenic genes: *TGFB1*, *CTGF*, *COL4A1* and *ACTA2* in cells in G0/G1 or G2/M phase (bottom) ($n$ = 3 experiments). $^{*}P < 0.001$, $^{**}P < 0.05$ versus control G0/G1; $^{\#}P < 0.001$, $^{\#\#}P < 0.05$ versus control G2/M; &$P < 0.01$ versus RO 48 h G2/M. (**d**) Cell cycle changes in HK-2 cells treated with paclitaxel at various doses for 24 h. ($n$ = 3.) $^{*}P < 0.001$. (**e**) The CTGF protein (top western blot) and mRNA levels of *TGFB1*, *CTGF*, *COL4A1* and *COL1A1* (bottom) in HK-2 cells treated with paclitaxel for 24 h. $n$ = 5. $^{*}P < 0.001$. For mRNA levels in **b** and **e**, control values were arbitrarily set to 1. (**f**) The cell cycle changes in proliferating tubular cells in moderate IRI models without (day 1) or with (>day 1) paclitaxel treatment. $^{*}P < 0.01$, $^{\#}P < 0.05$. Symbols in the cell cycle data graphs refer to the comparison of G2/M phases. (**g**) Masson's trichrome staining of moderate IRI kidneys with or without paclitaxel treatment (21 d after injury, $n$ = 3 mice in each group). Scale bar, 50

μm. (**h**) The serum creatinine changes in moderate IRI models with or without paclitaxel treatment. Error bars represent s.d.

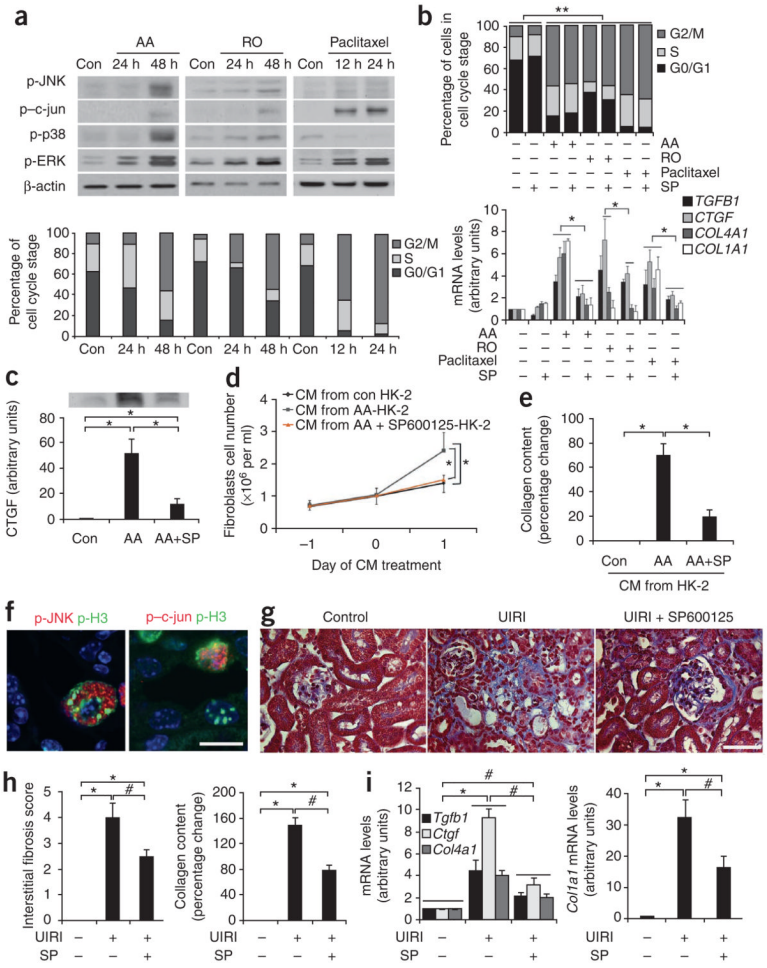


**Figure 6.**

JNK signaling activation mediates G2/M arrest–induced profibrogenic cytokines upregulation. (**a**) Western blot analysis of MAPK pathway activation (top) and the corresponding cell cycle distribution (bottom) of HK-2 cells treated with aristolochic acid, RO3306 or paclitaxel. ($n$ = 3–5.) (**b**) Effects of the JNK inhibitor (SP600125, SP) on cell cycle distribution (top) and profibrogenic gene expression (bottom) in HK-2 cells treated with aristolochic acid, RO3306 (RO) or paclitaxel. ($n$ = 3.) mRNA data are presented as fold induction over the untreated cells. *$P$ < 0.05, **$P$ < 0.001. Symbols in the cell cycle graphs refer to the comparison of G2/M phases. (**c**) The protein amounts of CTGF in the supernatant from HK-2 cells treated with aristolochic acid or aristolochic acid together with SP600125 (AA + SP) versus untreated cells (CON). Data are presented as fold induction over the control cells ($n$ = 3). *$P$ < 0.001. (**d**) The proliferation of fibroblasts incubated with conditioned medium (CM) from HK-2 cells treated with aristolochic acid or from HK-2 cells treated with aristolochic acid together with SP600125. ($n$ = 3.) *$P$ < 0.01. (**e**) The collagen content, expressed as percentage change over control, in the supernatant from fibroblasts incubated with CM from aristolochic acid–treated HK-2 cells or from HK-2 cells treated with aristolochic acid together with SP600125 (SP). ($n$ = 3.) *$P$ < 0.01. (**f**) Co-localization of p-JNK or p–c-jun with p–histone H3 in AAN kidney on day 7. Scale bar, 10 μm. (**g**) Masson's trichrome staining of UIRI kidneys with or without SP600125 treatment on day 28 after UIRI. Scale bar, 50 μm. (**h**) Quantitative kidney interstitial fibrosis score (left) and collagen content in the kidneys on day 28, as determined by the Sircol assay

(right). *$P < 0.001$, $^{\#}P < 0.05$. (**i**) Effect of JNK inhibition on profibrogenic gene expression in UIRI-treated kidneys. Data are presented as fold induction over the untreated cells. *$P < 0.001$, $^{\#}P < 0.05$. Error bars represent s.d.